Liquid Crystals
Publication details, including instructions for authors and subscription information:
http://www.informaworld.com/smpp/title~content=t713926090

Structure of organized organic mono- and multi-layer films

F. Rustichelli

Online publication date: 06 August 2010

To cite this Article Rustichelli, F.(1998) 'Structure of organized organic mono- and multi-layer films', Liquid Crystals, 24: 1, 39 — 48
To link to this Article: DOI: 10.1080/026782998207569
URL: http://dx.doi.org/10.1080/026782998207569

LIQUID CRYSTALS, 1998, VOL. 24, NO. 1, 39–48

Structure of organized organic mono- and multi-layer films

by F. RUSTICHELLI
Istituto di Scienze Fisiche, Università di Ancona, Via Ranieri, 65, 60131 Ancona, Italy
Istituto Nazionale di Fisica della Materia (UdR di Ancona)

Presented at the Capri Symposium in Honour of George W. Gray, FRS held at the Hotel Palatium, Capri, 11–14 *September* 1996

A review is presented of some interesting structural properties of monomolecular layers at the air/water interface (Langmuir films) and of supramolecular assemblies consisting of organized multilayer structures of organic molecules (Langmuir–Blodgett films). In particular multilayer films of bipolar lipids from archaebacteria and of proteins are considered, together with single-electron junction quantum effects in multilayers containing nanoparticles. In parallel, special emphasis is given to some recently developed experimental techniques based on X-ray scattering.

1. Introduction

The interest of the scientific community in organized monomolecular layers and supramolecular assemblies consisting of organized multilayered structures of organic molecules has been continuously increasing over the last decade, because of the implications of these systems both in fundamental and applied research.

Examples of applications of these layers in the fundamental field are found in the photophysical field and in the use of organized layers of lipids as models of naturally occurring cell membranes. On the other hand, organized molecular layers can find application in classical electronics as microlithographic resists (in the frame of development of faster and greater memory storage capacity in integrated circuits), magnetic tape lubrication, liquid crystal alignment, non-linear optics, biosensors and the early development of molecular electronic devices.

Historically, the investigation of monomolecular organic films began in the eighteenth century when Benjamin Franklin, during a visit to England, performed a simple experiment by putting small quantities of oil on the surface of a small lake and observing their quick spreading till interference colours appeared, with a simultaneous calming effect on the waves.

A widespread technique to prepare organized multilayered structures of organic molecules is the Langmuir–Blodgett (LB) technique, which allows the creation of arbitrary sequences of monolayers of different chemical compounds in a direction perpendicular to the substrate surface, i.e. of supramolecular organizations with molecular scale variations along this direction [1–12].

By using the LB technique, one can obtain systems which can be designed in the frame of so-called *molecular architecture* (figure 1 shows how LB films are related to other interesting natural and artificial supramolecular organizations). An example of such architecture can be found in reference [13] in which a sequence of alternating dielectric and conducting layers was obtained and investigated, as discussed below. In view of electronic device development, the discovery of field effects in conducting LB films [14] and of single-electron junctions at room temperature [15], involving single electron transfer, should be mentioned.

After a section devoted to a brief description of the preparation techniques of monolayers and multilayers, several examples will be presented of structural investigations of these supramolecular assemblies, including appropriate emphasis on recently developed experimental analytical techniques.

2. Preparation of Langmuir–Blodgett films

2.1. *Monolayers at the air/water interface (Langmuir films)*

When a solution of amphiphilic molecules in a water immiscible solvent (e.g. chloroform) is spread on a liquid surface (typically water), a monomolecular layer is formed (called a Langmuir film), where the molecular head groups are immersed in the water surface and the tails remain outside.

If the interactions between the molecules are weak (i.e. the distance between the molecules is large), the monolayer can be considered as a two-dimensional gas. Under these conditions, the effect of the monolayer on the water's surface tension is relatively little. It is possible

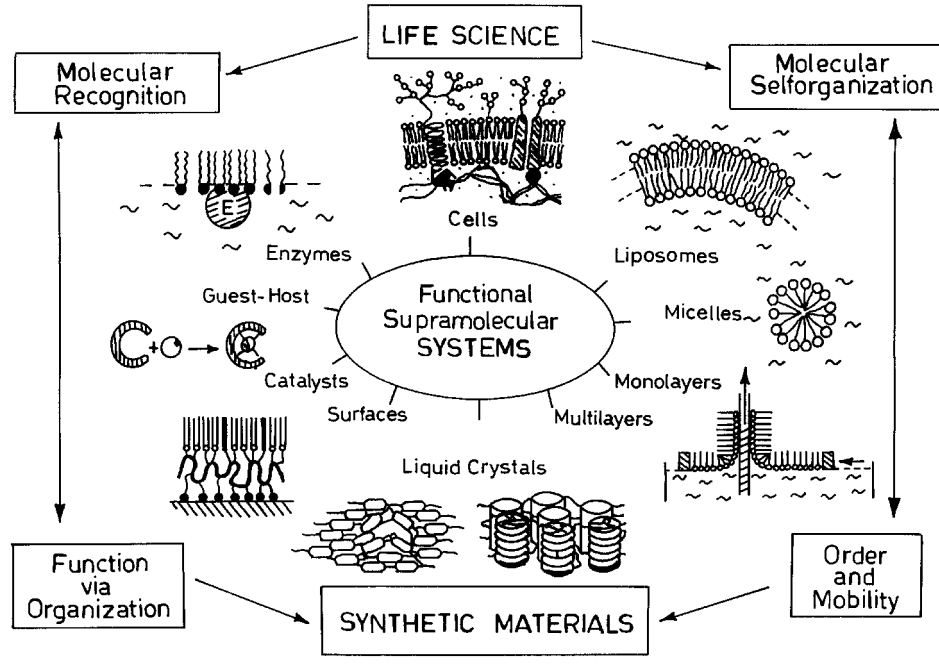

Figure 1. Schemes of different natural and artificial functional supramolecular systems [38].

to reduce the area available for the monolayer using a mobile barrier system: during compression the molecules exert a repulsive effect on each other, related to the surface pressure.

The plot of the surface pressure as a function of the area available per molecule, recorded at a constant temperature, is known as the 'surface/pressure isotherm'. Curves of this kind are usually obtained by very low compression of the monolayer itself, at a constant rate, and they can be considered as a sequence of pseudo-equilibrium states.

A typical surface/pressure isotherm is reported later in the insert of figure 8. A number of distinct regions can be considered, corresponding to different intermolecular organizations and molecular conformations. For large surface area values and low surface pressure values ($<1\,\mathrm{mN\,m^{-1}}$), the hydrophobic tails are lying near to the water surface and forming the so-called bidimensional gaseous phase. By reducing the value of the surface area, a first phase transition occurs to the liquid-expanded (LE) phase. By further reduction of the surface area, a second phase transition into a bidimensional 'solid' or condensed phase can be observed: the molecules are now closely packed, and the chains are stiff and uniformly oriented. If the monolayer is submitted to further compression, the phenomenon of collapse occurs and an abrupt decrease of the surface pressure is observed.

A typical device used to obtain Langmuir films is shown in figure 2. It consists of a Teflon rectangular trough, which is filled with the aqueous subphase, and it is usually equipped with one or two movable barriers allowing the monolayer compression. Other typical devices, commercially available, are, e.g. circular troughs [5] and constant perimeter barrier systems [6].

2.2. *Deposition of multilayer films (Langmuir–Blodgett films)*

The monolayer formed at the air/water interface can be transferred onto a solid substrate using what has become universally known as the Langmuir–Blodgett (LB) technique. In a typical experiment, the substrate (for instance a glass slide or a silicon wafer) is first lowered into the liquid subphase and then withdrawn. At each passage through the surface, the monolayer is transferred onto the solid substrate and by repeating the procedure several times, it is possible to build up ordered multilayers. A schematic diagram is reported in figure 2. Besides the described vertical deposition, another technique used to build up ordered multilayers is horizontal deposition, developed by Langmuir and Schaefer [7].

3. Small-angle X-ray diffraction

3.1. *Introduction to the technique*

Figure 3 (*a*) shows schematically the geometry of X-ray small-angle diffraction by an LB film recorded by a powder diffractometer. The diffracted intensity is recorded by rotating the sample by an angle θ and the detector by an angle 2θ. In a typical diffraction pattern, the detected X-ray intensity is recorded as a function of 2θ. Typically between 10 and 15 Bragg reflections are recorded, whose spacing ratios in the order 1:2:3:4:..., clearly indicate a one-dimensional lamellar symmetry corresponding to a stacking of the molecular layers.

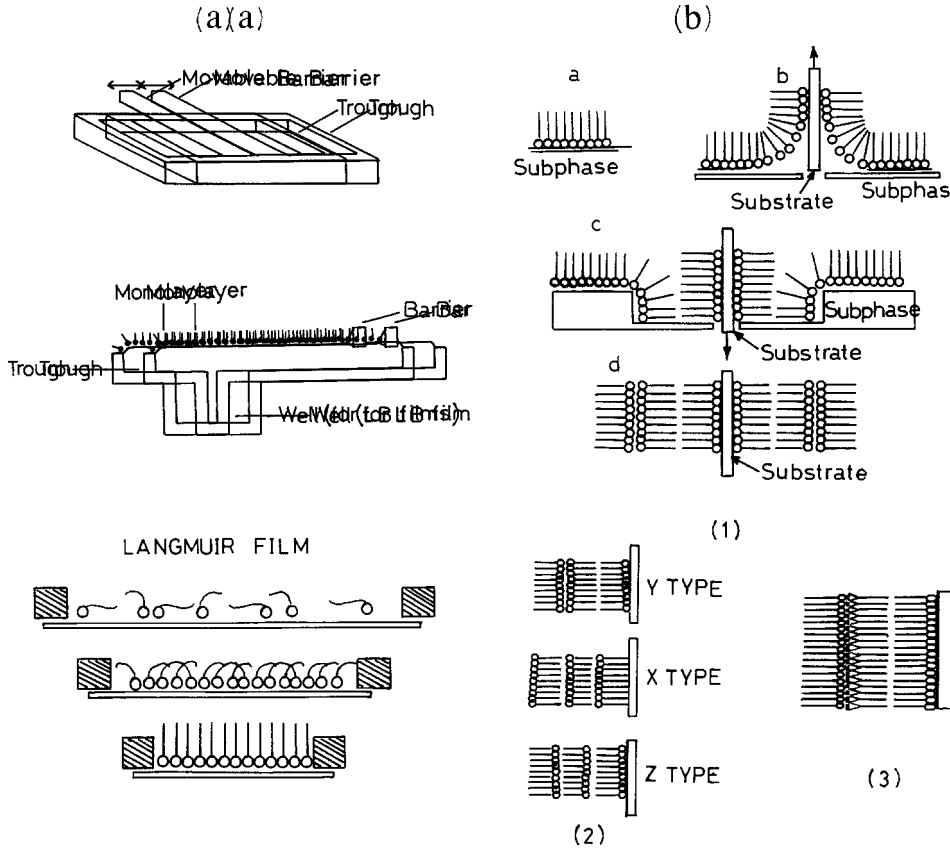

Figure 2. (*a*) Sketch of a device to obtain monolayers (Langmuir films) at the air/water interface. (*b*) Deposition of a multilayer film on a solid support by the Langmuir–Blodgett technique of deposition (1); different possible structures of the deposited multilayers are shown in (2); in (3) an example of *molecular architecture* is reported involving the deposition of three different monomolecular layers.

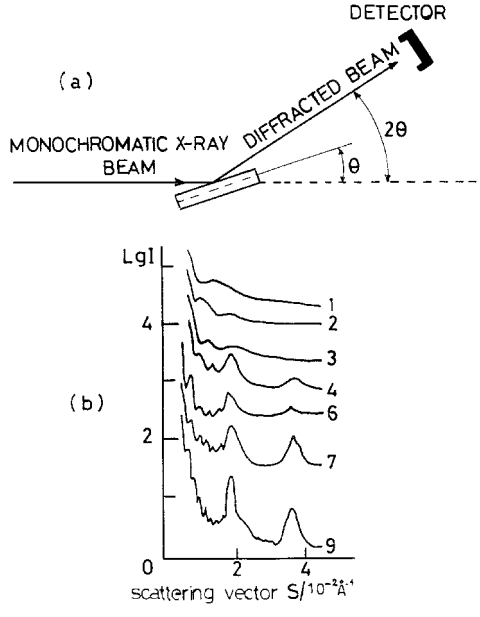

Figure 3. (*a*) X-ray small-angle diffraction by an LB film; (*b*) typical X-ray scattering patterns as a function of the number (labelling on each curve) of bilayers of Tl behenate [16].

Figure 3 (*b*) reports typical X-ray scattering patterns as a function of the number of bilayers of Tl behenate [16]. From the position of the Bragg peaks, by using the Bragg equation, one obtains the spatial periodicity of the supramolecular system. Furthermore one can obtain the electron density profile $\rho(z)$ along a direction perpendicular to the layers by traditional crystallographic methods.

3.2. *Multilayers of archaeal lipids*

Archaea are extremophilic micro-organisms, phylogenetically separated from Eubacteria and Eukarya, living in extreme environmental conditions such as high temperature, low pH or high salt concentration.

Lipids extracted from *Sulfolobus solfataricus*, a micro-organism growing optimally at 87°C and pH 3 have been intensively investigated [17–23]; these lipids possess a bipolar structure with two polar heads and a hydrophobic moiety of approximately double the average length with respect to that of the aliphatic chains of classical ester lipids contained in other living organisms. Due to this peculiar molecular structure, lipids from thermophilic archaea appear to be promising for producing artificial devices, stable at high temperature and

suitable for incorporating some functional molecules, e.g. proteins.

All the investigated compounds are bipolar derivatives of two dialkyl tetra-ethers, i.e. glycerol-dialkyl-nonitol tetra-ether (GDNT) and glycerol-dialkyl-glycerol tetra-ether (GDGT); some of them were obtained from naturally occurring materials by chemical modification of their polar heads, in order to obtain more stable monolayers [18].

In order to determine the conformation of the bipolar lipids inside the deposited mono- and multi-layers, low-angle diffractograms were recorded from an LB film of a semi-synthetic bipolar lipid named DS-GDGT [24]. Secondary maxima were observed between the Bragg peaks, from which the integral characteristics of the film, i.e. the number of layers and the overall thickness of the sample, can be obtained. These secondary maxima are associated with the one-dimensional periodic nature of the multilayer. In fact, as is well known [25], the intensity $I(q)$ diffracted by a film of N identical layers in the direction normal to the layer planes is given by the formula

$$I(q) = C|F_0(q)|^2 \frac{\sin^2(qNL/2)}{\sin^2(qL/2)} \qquad (1)$$

where $F_0(q)$ is the structure factor of the single layer, L is the thickness of the layer or, more precisely, of the periodic structural element, $q = 4\pi \sin\theta/\lambda$ is the modulus of the scattering vector normal to the layer planes (2θ is the scattering angle and λ is the wavelength of the X-ray beam) and C is a proportionality constant. The overall thickness $T = NL$ of the film can be calculated from the separation Δq between two adjacent zeros in the diffraction pattern (i.e. the oscillation period) as

$$T = \frac{2\pi}{\Delta q}. \qquad (2)$$

The number of molecular monolayers was assumed to be 40, according to the number of substrate insertions.

Figure 4 (*a*) shows the comparison between the experimental diffraction curve (thick line), after background subtraction and correction for the Lorentz and polarization factors, and the theoretical curve (thin line) calculated by means of equation (2) with $N = 19$. Very good agreement is observed over the whole range. This fact clearly indicates that the results are in agreement with the model reported in figure 4 (*b*), in which the molecules assume a U-shaped configuration and the L appearing in equation (1) corresponds to two molecular layers; therefore the number N of periodicities appearing in equation (1) is 19, i.e. approximately one half of 40, which is the number of the deposited molecular monolayers. An extended configuration for the lipid molecules would have produced a fringe separation higher by a factor of two as compared with those reported in figure 4 (*a*).

3.3. *Superlattices*

Reference [13] reports a successful result obtained in the production of artificial supramolecular assemblies at molecular scale spatial resolution. In fact an LB film was obtained and investigated consisting of a sequence of two dielectric bilayers of Ba stearate and one conducting bilayer of a binary mixture of hexadecyl-bis(ethylenedithio)tetrathiafulvalene ($C_{16}H_{33}$-BEDT-TTF) with 2-octadecylaminosulphonyl-tetracyanoanthraquinodimethane ($C_{18}H_{37}$-AS-TCNAQ). A superlattice periodicity of 148·7 Å was obtained from the several high order Bragg peaks observed in the X-ray diffraction pattern.

3.4. *Protein LB films and thermal stability*

Protein LB films are not easy to produce due to the non-amphiphilic nature of these biomolecules. A way of obtaining LB films of cytochrome C was to use as the spreading solution reversed micelles of sodium di-iso-octylsulphosuccinate (AOT), so encapsulating the proteins [26]. Figure 5 (*a*) reports the X-ray diffraction pattern from an LB film consisting of 10 periods (AOT-cytochrone C-AOT). The model obtained is reported in figure 5 (*b*), where the cytochrone C monolayer (circles) is placed between the head groups of AOT molecules in the adjacent monolayers.

LB films of other proteins belonging to the classes of metallo-proteins and immunoglobulins have been investigated. The first class is considered interesting for biomolecular electronics and the second for biosensors.

LB films of photosynthetic reaction centres from *Rhodobacter sphaeroides* (first class) and of anti-insulin antibodies from mice (second class) showed a much higher thermal stability compared with that of the proteins in solution. The reason for protein thermal stability in LB films (preservation of the secondary structure) is attributed to the close packing induced by LB film deposition [27].

3.5. *Quantum effects in LB films containing nanoparticles*

Mono-electron phenomena were recently observed at room temperature in nanometric particles of cadmium sulphide which were formed by exposing an LB film of cadmium arachidate to gaseous hydrogen sulphide [15]. Coulomb barrier and Coulomb staircase effects occur when a nanometric particle is connected to two electrodes by two tunnelling junctions: in this case a quantized increase takes place in the average number of electrons located on the particle, as a function of the increase of the bias voltage. In fact the electrons already

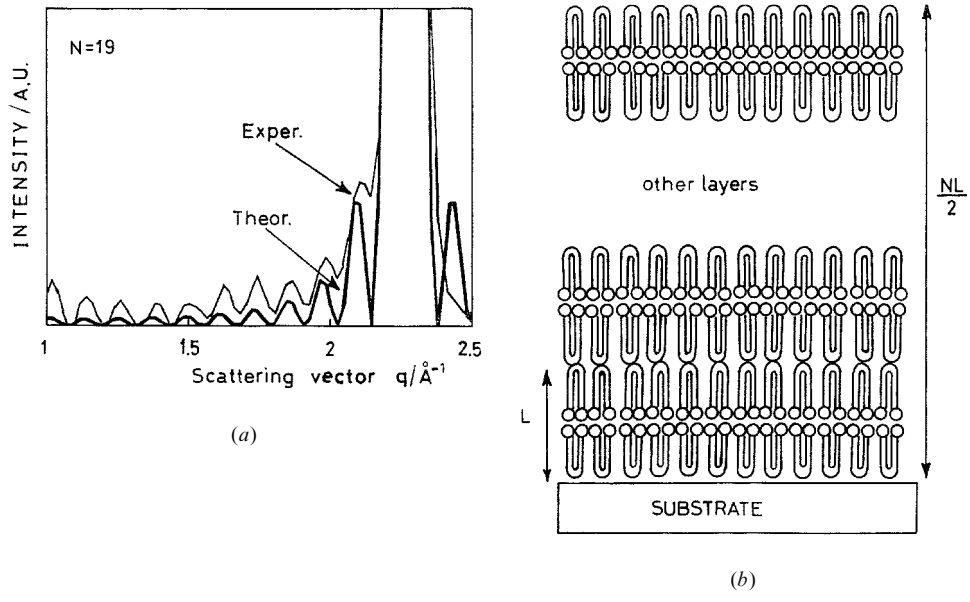

(a) (b)

Figure 4. (*a*) Small angle X-ray diffraction pattern of an LB film of DS-GDGT; the secondary maxima near the first order Bragg peak are reported. The figure shows the comparison between the experimental curve (thin line) and the theoretical curve corresponding to the U-shaped configuration of the lipids, as reported in (*b*) [24].

located on the particle produce an electric field which prevents an additional electron entering the particle until a sufficiently high voltage biases the junction.

The quantized increase in the average number of electrons occurs when the voltage through the structure increases by a quantity e/C, e being the electron charge and C the capacity of the system. As a consequence, the voltage–current characteristic shows a staircase behaviour [figure 6 (*a*)].

Figure 6 (*b*) shows how the data reported in figure 6 (*a*) were obtained: the LB film containing the CdS particles was produced directly on the tip of one electrode, thereby eliminating the need for using a scanning tunnelling microscope to identify the single nanoparticle and to perform the measurements there.

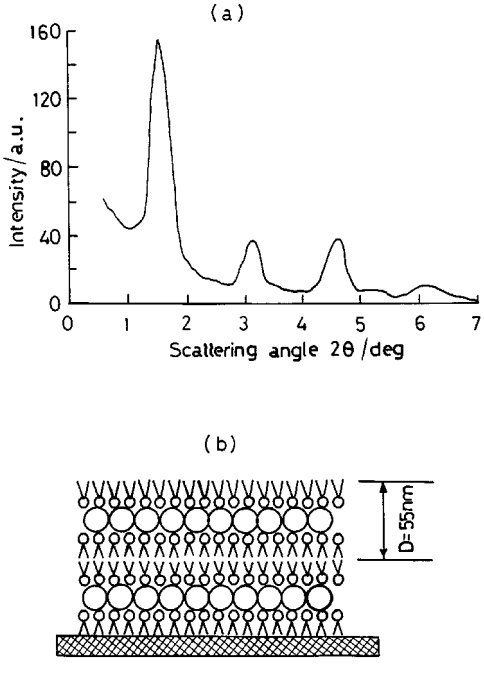

Figure 5. (*a*) X-ray diffraction pattern from an LB film consisting of alternating layers of an amphiphilic compound, sodium di-iso-octylsulphosuccinate (AOT) and of a protein, cytochrone C. (*b*) Model of the investigated LB film [26].

4. X-ray specular reflection

This technique (which is also called X-ray reflectivity at grazing incidence) provides electron density profiles along the direction normal to the surface, from which interesting structural information can be obtained in this direction on surfaces, interfaces and layers having thicknesses lower than several thousands of Å. In particular the molecular arrangement along the same direction can be obtained in Langmuir or LB films with a spatial resolution of a few Å. Moreover, surface and interface roughness and layer thickness can be derived.

Figure 7 reports schematically the geometry of the technique and of an X-ray diffractometer for liquids [28, 29]. An incident monochromatic X-ray beam of wavelength λ, (wave vector k_{in}), impinges on the sample surface at an angle θ and the reflected beam intensity, also at an angle θ, (wave vector $\mathbf{k}_{out}$), is recorded in the plane of incidence. As a consequence the scattering vector $\mathbf{q} = \mathbf{k}_{out} - \mathbf{k}_{in}$, which represents the exchanged wave vector, is perpendicular to the surface (figure 7).

In a typical experiment, a reflectivity profile defined as the ratio between the reflected and impinging X-ray intensity, $R(q)$, is obtained from the measured reflected intensity as a function of the incidence angle θ. For a single ideal diopter the reflectivity profile follows the

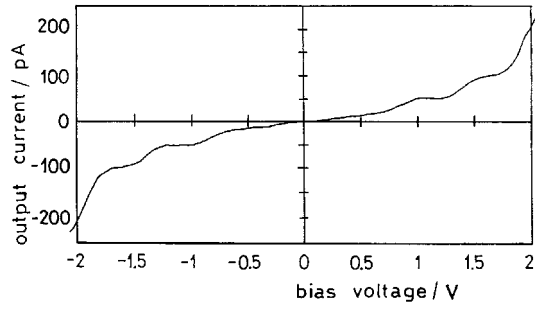

(*a*)

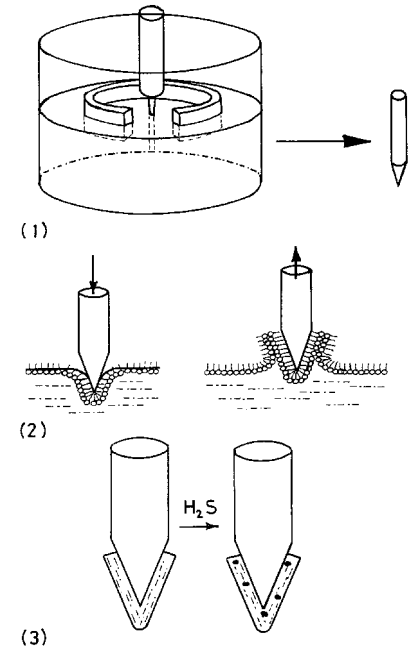

(*b*)

Figure 6. (*a*) Room-temperature voltage–current characteristics observed in nanometric particles of cadmium sulphide connected to two electrodes by two tunnelling junctions, as shown in (*b*). The step-like behaviour obtained is attributed to a quantized increase in the average number of electrons in a nanometric particle. (*b*) Scheme of the preparation of the sample for observing the quantum effect: (1) electrochemical etching of a tungsten stylus; (2) deposition on the stylus of a multilayer LB film of cadmium arachidate; (3) formation of CdS nanocrystals inside the LB film [15].

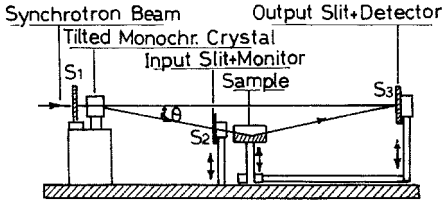

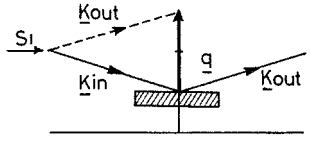

Figure 7. Experimental set-up for X-ray reflectivity from liquids, and the reciprocal space representation [28, 29].

Fresnel law

$$R_F(q) = (q_c/2q)^4 \qquad \text{for } q \gg q_c \tag{3}$$

q_c being the scattering vector associated with the critical angle of total reflection.

It can be shown that in general

$$R(q) = \frac{R_F(q)}{\rho_0^2}\left|\int \frac{d\rho(z)}{dz}\exp[iqz]\,dz\right|^2 \tag{4}$$

where $\rho(z)$ is the electron density profile perpendicular to the surface, $R_F(q)$ is the Fresnel reflectivity for an ideally sharp interface and $\rho_0{}^2$ is the electron density of the substrate.

Figure 8 reports the normalized X-ray reflectivity profiles R/R_F for L-α-dimyristoylphosphatidylethanolamine (DMPE) at different lateral pressures in a monolayer at the air/water interface as indicated in the isotherm of the insert. Region I corresponds to the liquid expanded phase (LE), region II to phase coexistence and region III to the solid phase [30]. The reflectivity profiles (*a*)–(*e*), including best fits, refer to the liquid expanded phase (LE), the profiles (*e*)–(*k*) refer to the phase coexistence range (the experimental points were replaced, for clarity, by smooth interpolating curves) and the profiles (*j*)–(*o*) refer essentially to the region associated with the solid phase.

The electron density profiles and the corresponding models, obtained from the best fits, for the solid phase and the fluid phase (LE), respectively, are reported in figure 9. For other structural information obtained, the reader should refer to reference [30]. X-ray reflectivity was also used to determine the structure of a Newton black film formed from sodium dodecylsulphate (SDS) solution in the presence of salt (NaCl) [31]. Figure 10 reports the electron density profile obtained along the normal to the film and the structural model. The film was much thinner than expected and did not contain any aqueous core, but only a hydration layer.

5. X-ray standing waves

The technique using X-ray standing waves is the most elegant and sophisticated among all the X-ray scattering techniques available at present. The standing waves, in

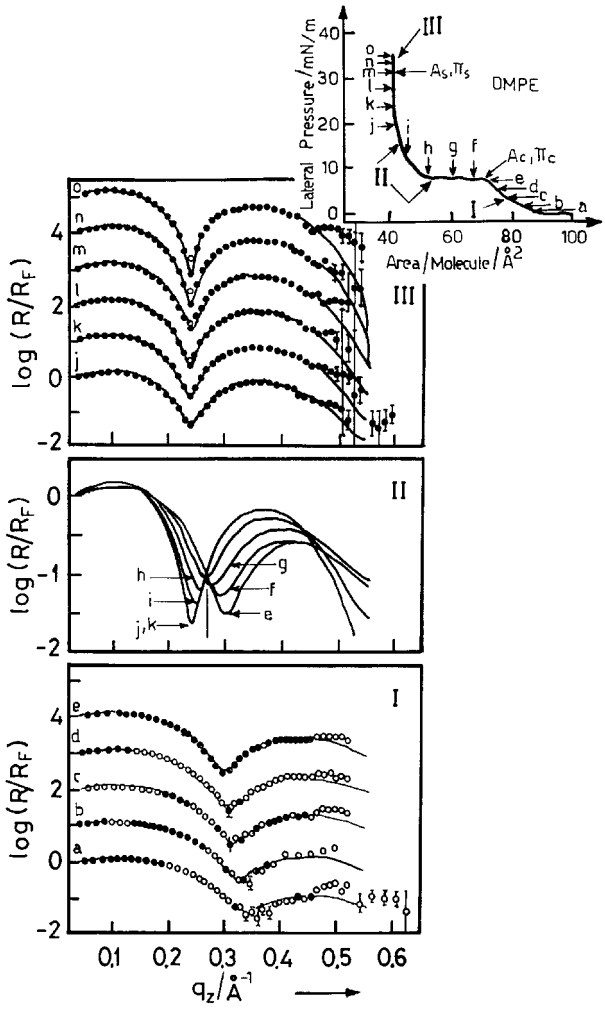

Figure 8. Normalized X-ray reflectivity profiles R/R_F for DMPE monolayers: the insert shows the point in the isotherm corresponding to the different profiles. (I) Liquid expanded (LE) phase range; (II) phase coexistence range; (III) solid phase range [30].

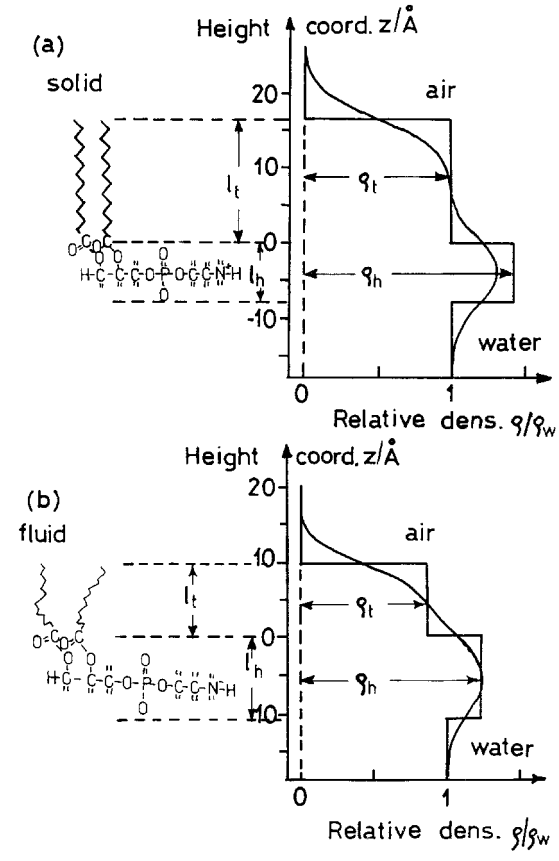

Figure 9. Electron density profiles and molecular conformations obtained from the reflectivity profiles of figure 8 for DMPE monolayers. (*a*) Solid phase; (*b*) liquid expanded (LE) phase. The following parameters are also defined: layer thicknesses l_h, l_t, and electron densities ρ_h, ρ_t, [30].

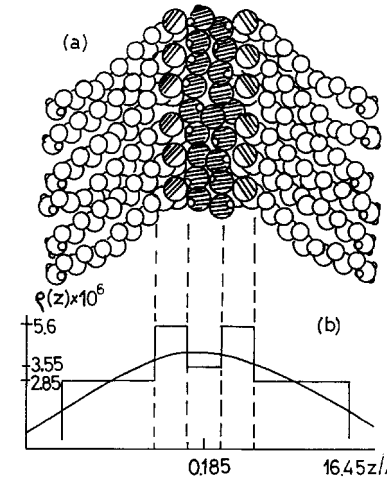

Figure 10. (*a*) Structural model of the film; (*b*) electron density along the normal to a Newton black film formed from a sodium dodecylsulphate (SDS) solution in the presence of NaCl [31].

the most recent applications, are the result of the interference between the incident, $\mathbf{E}_o$, and the specularly reflected, $\mathbf{E}_r$, plane waves (figure 11). The electric field intensity in the vacuum above the reflecting mirror surface can be written as [32, 33].

$$I(\theta, z) = |\mathbf{E}_O|^2 \{1 + R + 2[R\cos(\nu - 2\pi Qz)]^{1/2}\} \quad (5)$$

where $|E_o|^2$ is the intensity of the incident beam, R is the reflectivity, ν is the phase of the reflected beam relative to the incident beam, and

$$q = 2\sin\theta/\lambda = 1/D\,. \quad (6)$$

For a fixed value of q, i.e. of the incidence angle θ, the intensity $I(\theta, z)$ modulates between 0 and 4 $|\mathbf{E}_o|^2$, when $R = 1$ (total reflection region), producing a standing

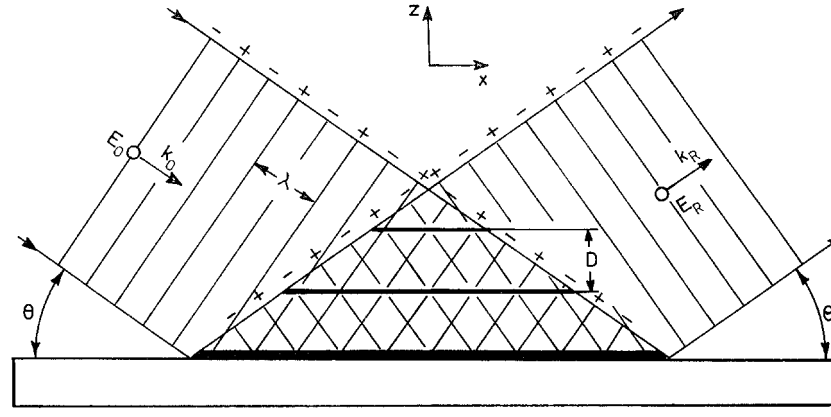

Figure 11. Sketch of the X-ray standing wave field arising from interference between the incident, $\mathbf{E}_O$, and specular-reflected, $\mathbf{E}_R$, plane waves above a mirror surface. The antinodes are represented and have a period $D = \lambda/2 \sin\theta$ [34].

wave, the antinodes of which are parallel to the mirror surface and have a spatial period of

$$D = \lambda/2 \sin\theta \qquad (7)$$

as indicated in figure 11. Since the total reflection condition occurs between 0 and θ_c, from equation (6) one finds that D varies from ∞ to $D_c = \lambda/2 \sin\theta_c$, i.e. in practice from 1000 to 100 Å. At $\theta = 0$, a standing wave node is at the mirror surface and the first antinode at infinity. When q is increased, as D decreases [equation (6)], the first antinode moves towards the mirror surface and practically coincides with it for $\theta = \theta_c$: the other nodes and antinodes of the standing wave also move inward. This technique can be used to evaluate the position of a heavy atom layer above the reflecting surface, by monitoring the fluorescence yield from that atom layer as a function of incidence angle θ. In fact the photoelectric effect signal is proportional to the E-field intensity at the centre of the given atom and it is clear that the fluorescence yield strongly depends on the position of the atom layer as compared with the position of the antinode, i.e. to the position of the reflecting surface. Heavy atoms can be located with Ångstrom or sub-Ångstrom resolution.

An LB film of lipids and a reference sample have been investigated by this technique [34]. The LB film (figure 12) (sample A) consists of a hydrophobic gold mirror with 14 bilayers of ω-tricosenoic acid (ω-TA) and an inverted bilayer of Zn arachidate, implying that the distance of the Zn layer above the Au mirror surface is ~926 Å. A reference sample (sample B) was prepared without the 14 ω-TA bilayers, implying that the Zn layer is ~42 Å above the surface. Figure 13 reports the experimental results, i.e. the fluorescence yield (*a*), the X-ray reflectivity profile (*b*) as a function of the incidence angle, and the zinc distribution obtained above the surface (*c*) for the sample A. Curves (*d*)–(*f*) show the same quantities, respectively for sample B.

The several peak maxima appearing in figure 13 (*a*)

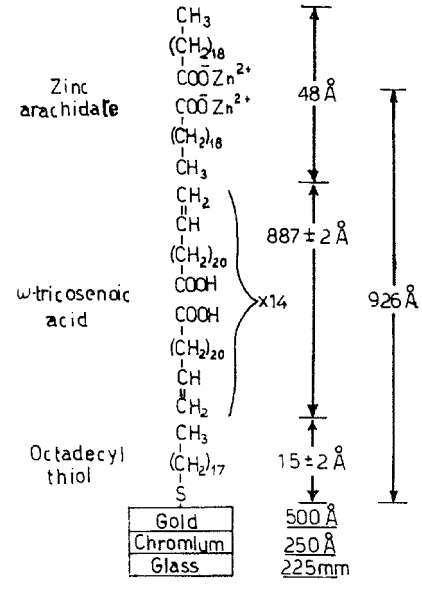

Figure 12. Sketch of the gold mirror and the deposited LB film investigated by the X-ray standing wave technique [34].

represent the crossing of antinodes of the X-ray standing wave with the Zn layer, when θ is increased, whereas the minima correspond to the crossing of nodes. In figure 13 (*d*) only one antinode is crossing the Zn layer, which is in fact much nearer to the mirror surface. Other investigations of LB films by the same technique can be found in references [35, 36]. Recently phase transitions in LB films have also been investigated (M. Caffrey, private communication). In conclusion this technique is very useful in surface structure investigation of, for example, protein films, and membrane–membrane and receptor–ligand interactions.

6. Surface diffraction

The surface diffraction technique (also called horizontal or in-plane diffraction, or grazing incidence X-ray

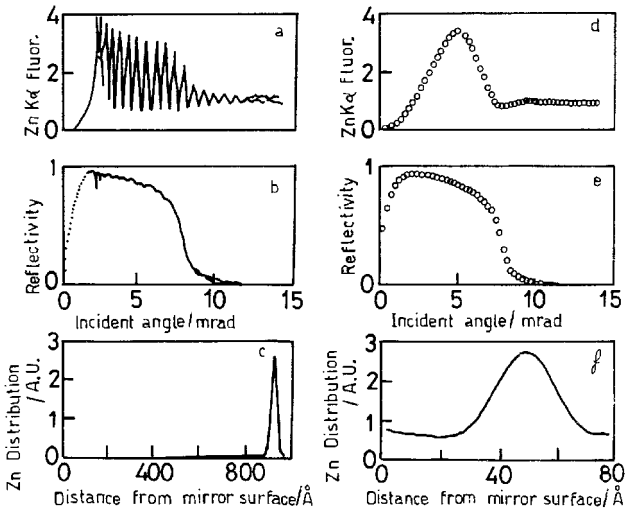

Figure 13. Experimental angular dependence of the Zn K_α fluorescence yield (*a*); specular X-ray reflectivity (*b*); and calculated Zn distribution above a Au surface for an LB film containing 14 bilayers of ω-tricosenoic acid and an inverted bilayer of Zn arachidate (*c*). The same quantities are reported in (*d*)–(*f*), respectively, for a reference sample without the 14 bilayers of ω-tricosenoic acid [34].

diffraction) is strictly related to the specular reflection technique, and its principle is sketched in figure 14. A highly collimated and monochromatic X-ray beam impinges on the air/water interface at a vertical angle α_i just under the critical angle of total reflection θ_c, and, if an in-plane periodicity inside the monolayer exists, is reflected at the angle α_f, corresponding to a 2θ deflection in the horizontal plane. In these conditions of total reflection ($\alpha_i < \theta_c$), an evanescent wave travels in a direction parallel to the interface. Its intensity decays exponentially along a direction perpendicular to the interface. The penetration depth Λ (figure 14), which depends on the incidence angle, is of the order ~ 100 Å. The evanescent wave is therefore diffracted by planes normal to the surface in a very thin region beneath the surface itself. From the position of the diffracted spot on

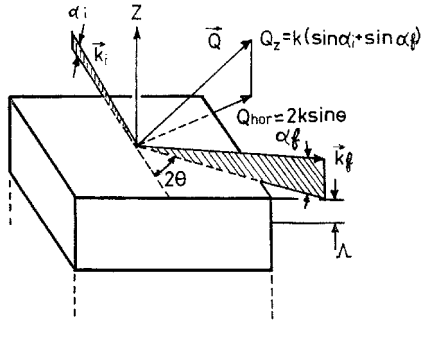

Figure 14. Geometry for surface diffraction with larger horizontal (Q_{hor}) than vertical (Q_z) scattering vector component [30].

a bidimensional multidetector, one can deduce, using Bragg's law, the spacing of the diffracting planes, and from the width of the spot, the correlation length ξ. Figure 15 reports the X-ray diffracted intensity as a function of the wave vector transfer Q for increasing lateral pressure (*a*)–(*b*), corresponding to the arrows of the pressure/area isotherm of the insert, for a phospholipid monolayer at the air/water interface [37].

Qualitatively, one can deduce a decrease in the interplanar distance from the shift of the peak to higher Q values, and an increase of the correlation length from the narrowing of the peak. Quantitatively, the correlation length ξ, the integrated X-ray intensity X, and the lattice spacing d, are reported in figure 16, as deduced from the data of figure 15.

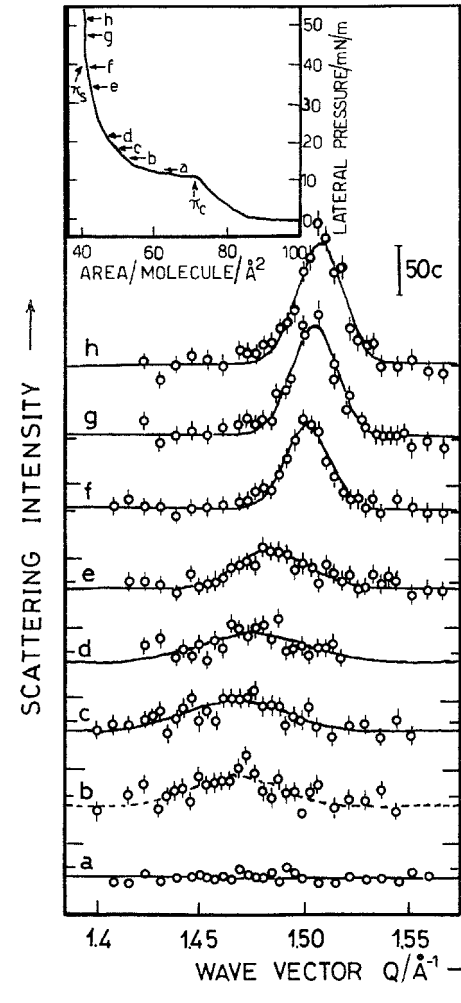

Figure 15. In-plane X-ray diffracted intensity as a function of wave vector transfer Q for increasing surface pressure (*a*)–(*h*) corresponding to the arrows in the insert. Monolayer of dimyristoylphosphatidic acid, pH 5·5, ionic content 10^{-2}M NaCl, 5×10^{-5}M ethylenediaminetetraacetic acid, $T = 19 \pm 2$°C [37].

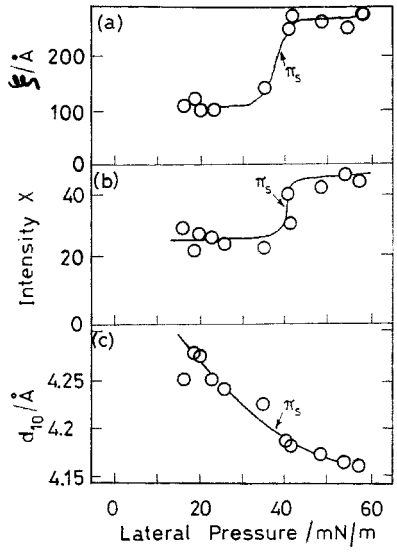

Figure 16. (*a*) Correlation length ξ, (*b*) integrated X-ray intensity, and (*c*) lattice spacing *d*, as function of lateral pressure for the dimyristoylphosphatidic acid monolayer of figure 15 [37].

7. Conclusions

The above reported experiments should provide evidence on the one hand that the construction of more and more intense X-ray synchrotron radiation sources and the development of new sophisticated X-ray scattering techniques allow us to obtain fundamental information on supramolecular organized layers, and on the other hand that these systems are also of great interest for several possible technological applications.

References

[1] Schwartz, D. K., Wiswanathan, R., and Zasadzinski, J. A., 1993, *Phys. Rev. Lett.*, **70,** 1267.

[2] Wiswanathan, R., Zasadzinski, J. A., and Schwartz, D. K., 1994, *Nature*, **368,** 440.

[3] Zasadzinski, J. A., Wiswanathan, R., Madsen, L., Garnaes, J., and Schwartz, D. K., 1994, *Science*, **263,** 1726.

[4] Roberts, G., 1990, *Langmuir-Blodgett Films* (New York: Plenum Press).

[5] Fromherz, P., 1975, *Rev. sci. Instrum*, **46,** 1380.

[6] Zilversmit, D. B., 1963, *J. Colloid. Sci.*, **18,** 794.

[7] Langmuir, I., and Schaefer, V. J., 1938, *J. Am. Chem. Soc.*, **60,** 1351.

[8] Blodgett, K. B., 1952, *Step gauge for measuring thickness by means of interference*, U.S. Patent 2 587 282.

[9] Mann, B., and Kuhn, H., 1971, *J. appl. Phys.*, **42,** 4398.

[10] Kuhn, H., 1983, *Thin Solid Films*, **99,** 1.

[11] Rustichelli, F., 1995, in *Neural Networks and Biomolecular Engineering to Bioelectronics*, edited by C. Nicolini (New York: Plenum Press).

[12] Proceedings of the 7th International Conference on Organized Molecular Films, Ancona (Numana) Italy, September 10–15 1995, edited by G. Gabrielli and F. Rustichelli: 1996, *Thin Solid Films* **284/285**.

[13] Berzina, T. S., Troitsky, V. I., Vorobyova, S. L., Feigin, L. A., Yasunova, L. G., Micheletto, R., and Rustichelli, F., 1992, *Thin Solid Films*, **210/211,** 309.

[14] Paloheimo, J., Kuivalainen, P., Stubb, H., Vyuorimaa, E., and Yei-Lahti, P., 1990, *Appl. Phys. Lett.*, **56,** 120.

[15] Facci, P., Erokhin, V., Carrara, S., and Nicolini, C., 1996, *Proc. Natl. Acad. Sci. USA*, **93,** 10556.

[16] Feigin, L. A., Lvov,, and Yu, M., 1988, *Makromol. Chem. Makromol. Symp.*, **15,** 259.

[17] De Rosa, M., Gambacorta, A., and Gliozzi, A., 1986, *Microbiological Reviews*, **50,** 70.

[18] Berzina, T. S., Troitsky, V. I., Vakula, S., Riccio, A., Gambacorta, A., De Rosa, M., Dante, S., Maccioni, E., Rustichelli, F., Accossato, P., and Nicolini, C., 1996, in *Molecular Manufacturing*, ELBA. Forum Series, Vol. 2, edited by C. Nicolini (New York and London: Plenum Press), p. 77.

[19] Dante, S., De Rosa, M., Maccioni, E., Morana, A., Nicolini, C., Rustichelli, F., Troitsky, V. I., and Yang, B., 1995, *Mol. Cryst. liq. Cryst.*, **262,** 191.

[20] Gulik, A., Luzzati, V., De Rosa, M., Gambacorta, A., 1985, *J. mol. Biol.*, **182,** 131.

[21] Berzina, T. S., Troitsky, V. I., Vakula, S. V., Riccio, A., Morana, A., De Rosa, M., Dante, S., Maccioni, E., Rustichelli, F., Accossato, P., and Nicolini, C., 1995, *Mat. Sci. Eng.*, **C3,** 13.

[22] Luzzati, V., Gulik, A., De Rosa, M., and Gambacorta, A., 1987, *Chemica Scripta*, **27B,** 211.

[23] Gulik, A., Luzzati, V., De Rosa, M., and Gambacorta, A., 1988, *J. mol. Biol.*, **201,** 488.

[24] Dante, S., De Rosa, M., Francescangeli, O., Rustichelli, F., Nicolini, C., and Troitsky, V. I., 1996, *Thin Solid Films*, **284/285,** 459.

[25] Guinier, A., 1963, *X-ray Diffraction in Crystals, Imperfect Crystals and Amorphous Bodies* (San Francisco: Freeman).

[26] Erokhin, V., Vakula, S., and Nicolini, C., 1994, *Thin Solid Films*, **238,** 88.

[27] Erokhin, V., Facci, P., and Nicolini, C., 1995, *Biosensors and Bioelectr.*, **10,** 25.

[28] Als-Nielsen, J., 1986, *Physica A*, **140,** 376.

[29] Benattar, J. J., Daillant, J., Belorgey, O., and Bosid, L., 1991, *Physica A*, **172,** 225.

[30] Heln, A., Tippman-Krayer, P., Möhwald, H., Als-Nielsen, J., and Kyaer, K., 1991, *Biophys. J.*, **60,** 1457.

[31] Belorgey, O., Benattar, J. J., 1991, *Phys. Rev. Lett.*, **66,** 313.

[32] Bedzyk, M. J., 1988, *Nucl. Instr. Methods*, **A266,** 679.

[33] Bedzyk, M. J., Bommarito, G. M., and Schildkrant, J. S., 1989, *Phys. Rev. Lett.*, **62,** 1376.

[34] Wang, J., Bedzyk, M. J., Penner, T. L., and Caffrey, M., 1991, *Nature*, **354,** 377.

[35] Zheludeva, S. I., Lagomarsino, S., Novikova, N. N., Kovalchuk, M. V., and Scarinci, F., 1990, *Thin Solid Films*, **193/194,** 395.

[36] Zheludeva, S. I., Kovalchuk, M. V., Novikova, N. N., Sosphenov, A. N., Erokhin, V., and Feigin, L., 1993, *J. Phys. D. appl. Phys.*, **26A,** 202.

[37] Kjaer, K., Als-Nielsen, J., Helm, C. A., Laxhuber, L. A., and Möhwald, H., 1987, *Phys. Rev. Lett.*, **58,** 2224.

[38] Ringsdorf, H., 1994, *Supramolecular Science*, **1,** 5.